PERGAMON

Deep-Sea Research II 46 (1999) 2877–2908

DEEP-SEA RESEARCH
PART II

A coupled 1-D biological/physical model of the northeast subarctic Pacific Ocean with iron limitation

K.L. Denman*, M.A. Peña

Institute of Ocean Sciences P.O. Box 6000, Sidney, BC, Canada V8L 4B2

Received 8 January 1998; received in revised form 29 September 1998; accepted 29 September 1998

Abstract

The recent NE subarctic Pacific study of the Canadian JGOFS project was designed primarily to address why phytoplankton biomass and production at Ocean Station Papa (OSP: 50°N, 145°W) are not as high as the nitrate concentrations could potentially support. To examine the possible role of iron (Fe) limitation in concert with microzooplankton grazing and physical supply of nitrate, we have coupled a four-compartment Nitrogen–Phytoplankton–Zooplankton–Detritus planktonic ecosystem model with a 60-layer (each 2 m thick) one-dimensional mixed-layer model (Mellor–Yamada level 2.5), driven by annual forcing characteristic of OSP. Both the physical and ecological models are forced with the same annual heat budget, mean phytoplankton concentration was tuned with the equilibrium solution of the model, and the zooplankton parameter values were chosen to be representative of microzooplankton. Modelled sea surface temperature ranged between 6 (fixed – late winter) and 13–14°C, depending on the distribution and amount of phytoplankton and detritus calculated by the model. Simulations with Fe limitation reducing the maximum specific growth rate of phytoplankton (for Fe-replete conditions) by a factor of ~ 3 best reproduced the annual cycle of surface layer nitrate, although the resulting annual *f*-ratio calculated from the fluxes into and out of the nitrogen compartment was marginally higher than recent estimates of *f*-ratio based on observations at OSP. The best simulations with Fe limitation agreed with observations of the annual cycle of surface nitrate concentration, the *f*-ratio, particulate nitrogen concentration in the euphotic layer, the export production, and the remineralization depth scale for sinking detritus, to within $\sim 50\%$, probably within the range of observational uncertainty and/or seasonal and interannual variability. Possible modifications include separating the detrital pool into suspended and sinking organic matter, decreasing the rate of remineralization with increasing depth, and examining the supply of nitrate to the surface layer by means of

* Corresponding author. Fax: + 1-250-363-6746.
E-mail address: denmank@pac.dfo-mpo.gc.ca (K.L. Denman)

PII: S0967-0645(99)00087-9

horizontal advection. The observational basis required to formulate these processes is marginal at present.

1. Introduction

The NE subarctic Pacific Ocean is a high nutrient-low chlorophyll (HNLC) oceanic regime with markedly different planktonic communities and ecosystem dynamics from those in the NE Atlantic Ocean (e.g., Parsons and Lalli, 1988). The NE subarctic Pacific Ocean has no pronounced spring bloom in phytoplankton biomass, and surface nitrate does not become depleted in summer, dropping to only about half its late winter maximum concentration. Superimposed on the seasonal cycle is considerable interannual varibility in nitrate concentrations and mixed-layer conditions, including evidence of long-term trends (Freeland et al., 1997; Whitney and Freeland, 1999). Hypothesized causes for the low seasonal variability and HNLC conditions in the NE Pacific (e.g. Miller et al., 1991; Chisholm and Morel, 1991) include significant winter primary production because of shallow winter mixing resulting in sufficient overwintering of zooplankton to graze down the spring increase in primary production, continuous high grazing capability by microzooplankton, and most recently, Fe limitation of phytoplankton growth that allows summer mixed-layer nitrate concentrations to remain well above limiting values.

Martin and Fitzwater (1988) and Martin et al. (1989) presented the first evidence that addition of Fe to water from OSP stimulated growth of phytoplankton and nitrate utilization, although interpretation of the in vitro Fe addition experiments was questioned because the containers were free of grazers (Banse, 1991). Boyd et al. (1996) found that in vitro Fe enrichment of water from OSP stimulated the growth of phytoplankton, even in the presence of micro- and mesozooplanktonic grazers. However, Tortell et al. (1996) and Maldonado and Price (1999) found that heterotrophic bacteria appear to account for 20–70% of the biological Fe uptake at OSP. Because neither the mechanisms of Fe cycling within the planktonic ecosystem nor the sources or sinks of dissolved Fe concentrations in the oceans are yet well understood (Martin and Gordon, 1988; Johnson et al., 1997), the NE subarctic Pacific study of the Canadian JGOFS project was designed primarily to test the hypothesis that Fe controls major aspects of the planktonic ecosystem at OSP (Boyd et al., 1999; overview). We present here results of a coupled one-dimensional (1-d) mixed layer/ecosystem model developed as part of the CJGOFS study to integrate the observational studies.

Starting with the bulk model of Denman (1973) and Denman and Miyake (1973), many mixed-layer models and ecosystem models have been developed for OSP, because of the long data series and because of the belief that mixed-layer and ecosystem dynamics there both might be little affected by horizontal advection. Evans and Parslow (1985), Frost (1987,1993), and Fasham (1995) all addressed aspects of grazing control of primary production with models ranging from three-component PZN models to the seven-compartment model of Fasham et al. (1990). Matear (1995)

applied parameter optimization techniques to three different ecosystem models of OSP and found that there were insufficient observations from OSP to constrain a seven-compartment model. In all these ecosystem models the mixed layer was represented by a prescribed annual cycle in depth and a specified mixing rate between the mixed layer and the ocean below. Two studies have employed coupled 1-d mixed-layer/ecosystem models. Kawamiya et al. (1995) compared a seven-compartment ecosystem model coupled with a 1-d mixed layer model with OSP observations, where observed sea-surface temperature was applied as a boundary condition. McClain et al. (1996) developed a coupled mixed-layer/ecosystem model to explore long-term changes in annual primary production in response to changes in wind, windstress curl (Ekman upwelling), and surface heating. Several other coupled 1-d mixed layer models have been applied primarily to surface layer CO_2 and O_2 cycling at OSP (e.g. Garçon et al., 1992; Thomas et al., 1993; Archer et al., 1993; Antoine and Morel, 1995a,b; Prunet et al., 1996a,b). None of these models however, specifically addresses the mechanisms of Fe limitation of macronutrient utilization.

In the equatorial Pacific, Frost and Franzen (1992) simulated possible Fe limitation with a model chemostat, and concluded that both Fe limitation and grazing control of phytoplankton biomass were required to simulate HNLC conditions; Fe limitation alone was insufficient. Chai et al. (1996) investigated Fe limitation in the equatorial Pacific with an ecosystem model embedded in an ocean general circulation model. They simulated Fe enrichment/supply by increasing the initial slope of the photosynthesis–light relationship and the maximum specific growth rate of phytoplankton, relative to their 'standard' simulations. They too concluded that while physiological (i.e. Fe) limitation plays a significant role in the maintenance of the high nitrate anomaly, physical processes and grazing are also involved. Loukos et al. (1997) developed an ecosystem model that included a conservation equation for Fe for the equatorial Pacific, where there is a greater knowledge of in situ Fe concentrations. Their simulations demonstrated that Fe supply controls primary production variability but grazing balances primary production and controls phytoplankton biomass.

Cullen (1995), in an examination and reformulation of the Fe hypothesis, also emphasized the essential role of grazing control (maintaining small phytoplankton at low concentrations and recycling ammonium), acting in concert with Fe limitation (maintaining diatoms at low concentrations). Landry et al. (1997) confirmed this view, and pointed out that nitrate uptake is strongly correlated with increasing pigment biomass of diatoms. They further suggested that HNLC regions function in essentially the same way as do oligotrophic subtropical regions, except that the limiting substrates differ.

To simulate the planktonic ecosystem at OSP and to examine the Fe-limitation hypotheses, we have embedded a four-compartment nutrient–phytoplankton–zooplankton–detritus planktonic ecosystem model in a 60-level 1-d mixed layer model (Mellor–Yamada level 2.5), driven by annual forcing characteristic of OSP. Both the physical and ecological models are forced with the same annual heat budget, i.e. sea surface temperature is an output, not a boundary condition of the model. In particular, we report on the results of model simulations examining the following aspects of plankton ecosystem functioning at OSP: (i) a scenario by which Fe limitation could

affect ecosystem processes at OSP, (ii) the strong effect of sinking organic detritus on surface-layer nitrate concentrations, (iii) the manner in which subsurface addition of nitrate (e.g. Ekman upwelling) affects surface-layer nitrate concentrations, and (iv) the relative importance of the fraction of primary production, grazing, and creation and remineralization of sinking organic detritus that occurs below the mixed layer during ~ 8 months of the year.

2. Physical mixed-layer model and forcing

We have chosen a Mellor–Yamada level 2.5 (MY2.5) model (Mellor and Yamada, 1974,1982) to couple with our biological model. MY2.5 models employ a version of the turbulent kinetic energy equation to estimate at each time step a turbulent length scale and vertical profiles of turbulent mixing coefficients for mass and scalars like temperature. Each time step, vertical mixing is performed by efficient implicit numerical algorithms: we use the same algorithm that mixes the temperature and salinity fields to mix the nitrogen, phytoplankton, zooplankton and detritus fields in the biological model. Martin (1985) and Large et al. (1994) used observations from OSP to evaluate and compare various mixed-layer models, including MY2.5 models similar to that used here. They found that MY2.5 models tend to produce a summer mixed layer that is too warm and too shallow, so we have employed a background diffusivity of 10^{-5} m^2 s^{-1}, which is five times that used in the simulations of Martin (1985) (included in the comparisons of Large et al., 1994). Matear and Wong (1997) recently estimated the vertical diffusivity just below the mixed layer at OSP to be 1.5×10^{-5} m^2 s^{-1}, from vertical distributions of chlorofluorocarbon. Zahariev (1998) determined that a background vertical diffusivity of $0.9–1.1 \times 10^{-5}$ m^2 s^{-1} best represented enhanced mixing by non-breaking internal waves ("heaving") in mixed-layer models of OSP. Martin (1985) found that a 20-fold change in background diffusivity in MY2.5 changed the simulated monthly SST at OSP by a maximum of 1.5°C.

Kantha and Clayson (1994) implemented a more complicated remedy to the undermixing of MY2.5 models, but in Large et al. (1994) their model yielded summer sea surface temperatures cooler than observations. Initially, we performed the simulations presented in this paper using a simple convective mixed-layer model (described in Denman and Gargett, 1995; Davis and Steele, 1994) that was forced with the daily and annual solar radiation cycles and a constant surface heat loss that balanced the annual solar heat input. Although that model had no wind mixing, the ecosystem results were not significantly different from those presented here.

The model domain is 120 m deep, divided into 60 2-m thick layers. A depth of 120 m represents the typical maximum depth of winter mixed-layer deepening at OSP (McClain et al., 1996; Whitney and Freeland, 1999), where the permanent halocline presents a barrier to deeper mixing, unlike at similar latitudes in the western North Pacific or in the North Atlantic. In addition, 120 m is well below the deepest 1% light levels (taken as the base of the euphotic zone) observed during primary production studies at OSP (e.g., Welschmeyer et al., 1993; Boyd et al., 1995a). We start the coupled model at the end of winter (1 March) with completely mixed conditions (6°C, 32.5 ppt).

Clear-sky solar radiation is calculated each time step (15 min) based on astronomical equations (Iqbal, 1983; Spencer, 1971; Lean, 1991). A constant cloudiness of 7 octas is assumed with the linear coefficients from Table 5 of Dobson and Smith (1988), although their climatology indicates slightly higher cloudiness in summer months. A constant sea-surface reflectivity of 6% is applied. Constant heat losses from the sea surface are adjusted to balance the solar heating over an annual cycle. We obtain an annual average solar input of 120.1 W m^{-2}, compared with the heat budget result of 112.5 W m^{-2} estimated by Dobson and Smith (1988) for the years 1959–1975. If we used a higher cloudiness in summer (requiring interpolating the constants in their table for fractional cloudiness values), we could improve the agreement with observations.

The solar radiation that provides the heating upon entering the ocean is divided into a long wave fraction (0.6) and a short wave fraction (0.4). The short wave fraction is also the photosynthetically available radiation (I_{PAR}) that supports primary production in the biological model. The long wave fraction is all absorbed in the first 2 m thick layer, while the I_{PAR} is absorbed throughout the water column. In most biological models the attenuation coefficient for I_{PAR} is obtained from a downward integration from the surface with some fraction dependent on the amount of phytoplankton chlorophyll *a* at each depth (see Evans and Garçon, 1997). However, at OSP such a formulation would not yield any significant annual cycle in underwater I_{PAR} because the depth-integrated (0–50 m) chlorophyll *a* does not have an annual cycle. Beam attenuation at a single wavelength correlates well with total particulate organic carbon in the NE subarctic Pacific (Bishop, 1998; Bishop et al., 1999), suggesting that attenuation of incident solar radiation may be affected by both phytoplankton and detritus. Thus, for the attenuation coefficient of I_{PAR}, $k_t(z)$, we use a modification of the linear formulation used by Evans and Parslow (1985) and Fasham (1995):

$$k_t(z) = k_w + k_c(P(z) + D(z)), \tag{1}$$

where k_w is the attenuation coefficient of sea water, and k_c is a single coefficient providing shading by both phytoplankton P and detritus D.

We used a spline interpolation of monthly COADS winds for OSP to obtain daily wind speeds and a constant drag coefficient of 1.3×10^{-3} to obtain an annual cycle in wind stress to force the model (minimum monthly mean wind speed of 6.79 m s^{-1} in July; maximum of 11.85 in December). The simulated mixed layer extends to the base of the model (120 m) for most of March, analogous to the penetration of the winter mixed layer at OSP to the top of the permanent halocline. The mixed-layer temperature (at midnight) varies annually between 6 and 13°C, again similar to the long-term mean annual cycle observed at OSP (McClain et al., 1996; Whitney and Freeland, 1999).

3. Biological model

3.1. Mathematical formulation

The NPZD biological model, consisting of four compartments, nitrogen N, phytoplankton P, microzooplankton Z, and detritus D, is shown schematically in Fig. 1. We

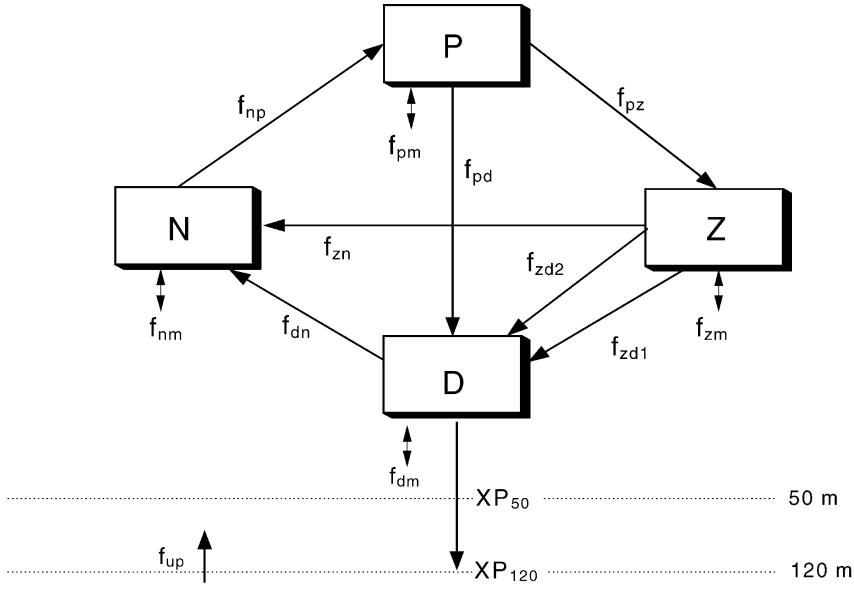

Fig. 1. Schematic diagram for the NPZD ecosystem model. Fluxes from compartment A to compartment B are denoted by the symbol f_{ab}, mixing flux of A across the 50-m level (f_{am}) are shown with double ended arrows (positive upwards). The export of sinking detritus across the 50-m level and out of the model domain is denoted by XP_{50} and XP_{120}. The addition of nitrate in the bottom 5 layers is denoted as f_{up}.

use nitrogen as our 'currency', so N consists of nitrate, ammonium and urea. The model is similar to that of Doney et al. (1996). The arrows in Fig. 1 represent the fluxes between the model compartments, and the subscripts denote the path of each flux. The double-ended arrows represent mixing fluxes across the 50-m horizon (+ ve upwards). For example, the primary production is labelled as f_{np}, denoting a flux from N to P, and the mixing flux across 50 m of Z is labelled as f_{zm}. XP_{50} and XP_{120} represent the export fluxes of sinking detritus D across the 50- and the 120-m horizon, the bottom of the model domain. The phytoplankton do not sink in this model, based on observations that (i) diatoms comprise less than 15% of the phytoplankton population biomass (Booth et al., 1993; Thibault et al., 1999) and (ii) during March, May and August 1996, cell sinking rates were negligible (0.01–0.59 m d^{-1}) and phytoplankton, as determined from pigment ratios, were healthy year round (Thibault et al., 1999).

The formulation of the fluxes between the model compartments is given in the set of four coupled ordinary differential equations that define the model:

$$\frac{dP}{dt} = (\text{growth})P - (\text{grazing})Z - m_{pd}P, \tag{2}$$

$$\frac{dZ}{dt} = g_a(\text{grazing})Z - (m_{zn} + m_{zd})Z, \tag{3}$$

$$\frac{dN}{dt} = -(\text{growth})P + m_{zn}Z + r_e D, \tag{4}$$

$$\frac{dD}{dt} = (1 - g_a)(\text{grazing})Z + m_{pd}P + m_{zd}Z - r_e D + w_s\frac{dD}{dz}, \tag{5}$$

where

$$\text{growth} = v_m \min\left\{\left(\frac{N}{k_n + N}\right), (1 - \exp(-\alpha I_{PAR}/v_m)), L_{Fe}\right\}, \tag{6a}$$

and

$$\text{grazing} = r_m \frac{P^2}{k_p^2 + P^2}. \tag{6b}$$

Under the assumption that only one factor limits phytoplankton growth at any time, the rate of phytoplankton growth is determined by the minimum value (evaluated each time step) of three functions, each ranging between 0 and 1, representing limitation by N, I_{PAR}, or Fe. Rather than taking the minimum (or threshold) in (6a), some investigators prefer to multiply the respective limitations on growth or uptake by nutrients and irradiance. When both factors are suboptimal, model results are sensitive to the formulation used (e.g. Haney and Jackson, 1996), but which formulation is more correct is still an open question requiring further experimental work (Cullen et al., 1993; Haney and Jackson, 1996). The nitrogen uptake is given by the usual Michaelis–Menten (Monod) function, and the light function derives from Webb et al. (1974).

Although Boyd et al. (1996) found phytoplankton growth rates in Fe-enriched carboys to be roughly twice those in the control carboys, and Maldonado et al. (1999), Maldonado and Price (1999), and Schmidt and Hutchins (1999) have all determined Fe : C uptake ratios for OSP, it is not possible either to develop a budget equation for Fe or to include its limiting effects by a Monod-like function because observations on annual cycles of in situ bioavailable Fe distributions and half-saturation values for Fe uptake in the subarctic Pacific are not yet available. Moreover, Tortell et al. (1996) and Maldonado and Price (1999) found that heterotrophic bacteria appear to account for 20–70% of the biological uptake of Fe at OSP. To complicate the picture further, Maldonado and Price (1999) have found evidence that natural assemblages of phytoplankton from OSP are capable of reducing Fe(III) bound in organic complexes and that both autotophic and heterotrophic plankton are capable of using these forms of Fe.

Thus, because a clear quantitative relationship between Fe supply and phytoplankton growth is yet to emerge, we have chosen to model its possible effect by a constant factor L_{Fe} that can reduce the growth rate of phytoplankton P. We will perform simulations with L_{Fe} taking on a series of values (constant in time) between 1 (no inhibition) and 0 (complete inhibition). As L_{Fe} is decreased, it will initially limit P only in summer when there is high irradiance, but as L_{Fe} takes on smaller values approaching 0, it could limit growth even in winter if it is smaller than the light function. We

realize that surface Fe concentrations should be greater in winter due to mixing from below the seasonal thermocline, but that increase may be offset in winter by the greater iron requirements of algae adapted to low light (Sunda and Huntsman, 1997; Maldonado et al., 1999). Accordingly, we have not specified an annual cycle in L_{Fe}.

Following the many studies showing that the dominant herbivores at OSP are microzooplankton (e.g. Landry et al., 1993; Booth et al., 1993), Z will be considered to consist primarily of microzooplankton. Phytoplankton are grazed by microzooplankton according to a standard quadratic grazing function (6b), referred to as a "Holling-type-III" predator response. The quadratic form of this grazing function at low values of P provides a threshold for grazing, considered to be a source of model stability (e.g. Steele and Henderson, 1992). Coupled with the linear mortality term for microzooplankton, the PZN dynamics are analogous to the model of Evans and Parslow (1985). Also, this combination of functions allows an analytic solution of the NPZD model (with no sinking) at equilibrium (Denman et al., 1998) which we use in setting initial values for some parameters.

The fraction of zooplankton grazing that is unassimilated, $(1 - g_a)$, (fecal pellets and 'sloppy feeding' material) flows to the detritus pool and is represented by the flux f_{zd2}. Other microzooplankton losses are partitioned between the dissolved nitrogen pool (f_{zn} representing regenerated nitrogen), and detritus (f_{zd1} representing dead body parts). The detritus pool D represents sinking, suspended and dissolved organic nitrogen (DON), characterized by a single average sinking rate w_s. The sinking detritus is remineralized back to the N pool at a rate r_e, representing implicitly the role of bacteria.

Since there is a sinking flux of detritus past a depth of 120 m (and out of the model domain), the model requires a physical supply of new nitrate, or it will eventually exhaust nitrogen (Denman and Gargett, 1995). We have simulated the supply of nitrate via Ekman upwelling f_{up} by adding a constant known amount of nitrate over the bottom five depth layers, which is slowly diffused upwards and finally entrained into the mixed layer as it descends each winter. Based on discussions at a recent JGOFS modelling workshop (Evans and Garçon, 1997), we initially had implemented a supply of nitrate via an Ekman upwelling speed of w_u (m y^{-1}) at the base of the model decreasing linearly to zero at the sea surface, such that it was divergent at all depths. Because the flow was everywhere divergent, we were unable to keep track of a budget for nitrate without considerable programming. The model behaviour was not altered significantly, and by changing to a simpler scheme we are now able to add a known amount of the macronutrient.

3.2. Selection of parameter values

The 'currency' of our model is nitrogen yet many observations are measured in units of carbon or chlorophyll *a*. For conversion between C and N, we use the Redfield value for C : N (atom : atom) of 6.6. For conversion between C and Chl, we use a constant value for C : Chl (wt : wt) of 60, based on the mean of the May–September observations of Booth et al. (1993) of 61.6 ($n = 134$). It is widely accepted that phytoplankton adapt to lower light conditions by reducing their C : Chl ratio, i.e.

Table 1
Model parameters for OSP simulations

Parameter	Symbol	Units	Value
PAR attenuation coefficient for sea water	k_w	m^{-1}	0.04
PAR attenuation coefficient for $(P + D)$	k_c	m^{-1} (mmol N m^{-3})$^{-1}$	0.06
Initial slope of P–I curve	α	d^{-1} (W m^{-2})$^{-1}$ [a]	0.08
Maximum phytoplankton growth rate	v_m	d^{-1}	2.0
Nitrogen half-saturation constant	k_n	mmol N m^{-3}	0.1
Phytoplankton mortality rate (to detritus)	m_{pd}	d^{-1}	0.05
Zooplankton maximum grazing rate	r_m	d^{-1}	1.0
Zooplankton assimilation efficiency	g_a	—	0.7
Zooplankton grazing half-saturation constant	k_p	mmol N m^{-3}	0.4
Zooplankton losses to nitrogen	m_{zn}	d^{-1}	0.20
Zooplankton losses to detritus	m_{zd}	d^{-1}	0.05
Detritus sinking speed	w_s	m d^{-1}	0, 3, 6, 10
Detritus remineralization rate	r_e	d^{-1}	0.1
Fe limitation value	L_{Fe}	—	0.1–1.0

[a] $d^{-1} \equiv day^{-1}$.

producing more Chl for light harvesting. However, the only winter values available come from Table 2 of Boyd et al. (1995a): total Chl (mg m^{-2}) ($n = 3$) over 0–80 m of 20–28, and total autotrophic C ($n = 2$) of 1600, giving a range for C : Chl of 57–80, with no indication of a lower ratio in (late) winter. Combining the two ratios, C : N and C : Chl, (and adjusting for the atomic weights of C and N) gives a ratio N(mmols) : Chl(mg) of 0.76. Thus, our target long term roughly constant phytoplankton biomass (average top 50 m) of 0.4 mg Chl m^{-3} (Wong et al., 1995) in N units should be 0.3 mmol N m^{-3}. The nitrogen compartment N is composed mostly ($\geqslant 95\%$) of nitrate (Wheeler, 1993; Whitney and Freeland, 1999) since regenerated forms are consumed rapidly by phytoplankton (Wheeler and Kokkinakis, 1990).

The parameter values used in the simulations presented here are given in Table 1. The depth attenuation coefficients for I_{PAR} (Eq. (1)) are those used by Fasham (1995), but shading is caused by D as well as P. The initial slope of the P–I curve, $\alpha = 0.08\ d^{-1}$ (W m^{-2})$^{-1}$ is taken from Evans and Parslow (1985), converted from $l\ y^{-1}$, with recent corroboration from Table 3 of Welschmeyer et al. (1993). They gave a mean α for 26 depth-integrated ^{14}C-experiments of 13.0 mg C (mg Chl)$^{-1}$ d^{-1} (Ein m^{-2} d^{-1})$^{-1}$. Using the conversion factor of Morel and Smith (1974) to convert from quanta to W m^{-2} and the C : Chl factor of 60, we obtain 0.078 d^{-1} (W m^{-2})$^{-1}$.

Welschmeyer et al. (1993) gave a range for maximum specific daily growth rates of surface, light-saturated phytoplankton assemblages of 0.59–1.38 d^{-1}. Therefore, we take the maximum instantaneous photosynthetic rate v_m as 2 d^{-1}, which for a 12-h day of saturated light conditions is equivalent to a value of 1 d^{-1}, representative of the range of observed values. The value used in this study of 0.1 mmol N m^{-3} for the nutrient half-saturation constant k_n is lower than in previous models but still higher than those estimated recently by Harrison et al. (1996). The phytoplankton mortality parameter m_{pd} is taken to be 0.05 d^{-1}, after Fasham (1995). The value of 0.7 for the

zooplankton assimilation efficiency coefficient g_a is the same as that of Doney et al. (1996), and similar to the value of 0.75 used by McGillicuddy et al. (1995) and Fasham (1995). A value of 0.4 mmol N m^{-3} for the half-saturation coefficient for zooplankton grazing k_p is roughly equal to that of Frost (1993) (0.52 mmol N m^{-3} after conversion) but 40% of that of Evans and Parslow (1985).

For parameters that do not correspond to quantities derived from observations, such as mortality or loss terms, we have used equilibrium solutions for the NPZD model that can be derived for the case with no nutrient addition and the detritus sinking speed set to zero, i.e. a closed system. We have simultaneously adjusted the values of k_p and the zooplankton losses $(m_{zn} + m_{zd}) = (0.20 + 0.05)\ d^{-1}$ in the equilibrium solutions to give a solution for phytoplankton biomass of 0.3 mmol N m^{-3} and a range of concentrations of zooplankton (over the seasons) that are of the same magnitude as the phytoplankton concentrations. Landry et al. (1993) and Boyd et al. (1995b,1996) found that grazing by microzooplankton nearly balances realized primary production when the phytoplankton consist primarily of small cells, a condition that appears to be prevalent at OSP most of the year: from dilution experiments phytoplankton growth rate (cruise averages) ranged 0.2–0.6 d^{-1}, the grazing rate, 0.2–0.5 d^{-1}, and the net growth rate 0.0–0.4 d^{-1}. If we take the maximum grazing rate by microzooplankton $r_m = 1\ d^{-1}$ and $k_p = 0.4$ mmol N m^{-3}, then the specific grazing rate, $r_m P^2/(k_p^2 + P^2)$, is $0.4\ d^{-1}$ when $P = 0.3$ mmol N m^{-3} and $0.7\ d^{-1}$ when $P = 0.6$ mmol N m^{-3}, comparable with observations of specific grazing rate, indicating that the modelled Zs are capable of maintaining grazing control. The partitioning of microzooplankton losses is somewhat arbitrary depending on the joint choice of parameters g_a, m_{zn} and m_{zd}.

As mentioned before, the detritus compartment contains non-living suspended and sinking PON and DON created by phytoplankton and zooplankton. The sinking (or non-sinking) of all these components is captured by a single sinking rate w_s, and their remineralization back to the inorganic nutrient pool by a single rate r_e. At depths where there are no biological source terms for detritus, Eq. (5) can be solved (in the steady state) for $D(z) : D$ decreases exponentially with depth z, with a depth scale of w_s/r_e m. In Table 2 we present nitrogen sinking fluxes for several-day deployments of

Table 2
Sinking PN fluxes for several-day deployments of drifting traps at OSP (Wong and Whitney, pers. comm.)

Month, 1996	PN flux, 100 m (mmol N $m^{-2}\ d^{-1}$)	PN flux, 200 m (mmol N $m^{-2}\ d^{-1}$)	w_s/r_e (m)	PN flux, 120 m (mmol N $m^{-2}\ d^{-1}$)
February	0.814	0.302	100	0.67
May	0.793	0.497	210	0.72
August	1.09	0.743	260	1.01

Derived values for the parameter group (w_s/r_e), and PN flux at 120 m, interpolated using the derived value for (w_s/r_e). (Last two columns use Eq. (5) with no inputs from P or Z.) The average of the three values in the last column, expressed as an annual flux, is 0.29 mol N $m^{-2}\ yr^{-1}$, which can be compared with the export flux at the bottom of the model, XP_{120} in Table 3.

drifting traps at OSP (Wong and Whitney, pers. comm.) From such fluxes we can estimate the remineralization length scale w_s/r_e to be 100, 210 or 260 m in February, May and August 1996. We set r_e to 0.1 d^{-1} after Doney et al. (1996), twice that of Fasham (1995) because we include non-sinking suspended particles and DON, which may 'remineralize' back to the inorganic nitrogen pool faster than sinking particles such as fecal pellets. We shall set the sinking rate to 0, 3, 6 and 10 m d^{-1}, yielding a maximum value for w_s/r_e of 100 m, the minimum value from the floating trap data in Table 2. Again, our justification is that since greater than half the organic material that we represent by D does not sink (e.g. Clegg and Whitfield, 1990; Charette et al., 1999). we need to use a shallower remineralization length scale and smaller sinking speeds than if D represented only particles that settle into drifting traps.

Based on thorium (^{234}Th) sorption on particles in the equatorial Pacific, Bacon et al. (1996) and Dunne et al. (1997) both estimated sinking speeds for organic particles from ~ 2 to ~ 20 m d^{-1} increasing with depth over the top 100 m. Dunne et al. (1997) also estimated remineralization rates of about 0.1–0.6 d^{-1} such that the remineralization length scale w_s/r_e may not be that different from our values. Charette et al. (1999) observed a thorium excess at OSP between ~ 150 and 200 m, suggesting that most remineralization, or at least redissolution of ^{234}Th, occurs over that depth range.

4. Simulations and results

The model was run for 3 or 5 yr for each standard simulation, with a time step of 15 min. The diurnal cycle in solar radiation is resolved, but we report midnight values for state variables and daily averages for fluxes. A "leap frog" time differencing scheme is used, with weak smoothing each time step to connect solutions between the even and odd time steps. Each simulation starts on 1 March (year day 60) at the end of winter, with the initial values $N_0 + P_0 + Z_0 + D_0 = 15$ mmol N m^{-3}. For the range of parameter values used in the biological model, the coupled model 'spins up' within a couple of months. For the balanced heat budget that we apply, sea-surface temperature and mixed layer P, Z, and D all repeat annually to at least 4 significant figures (when there is excess N). Three basic experiments were performed with the model. First, we investigated the effects of increasing the detrital sinking speed w_s; second, we investigated the effect of adding nutrients near the bottom of the model domain; and finally, we investigated a possible scenario by which Fe limitation might operate in the NE subarctic Pacific Ocean.

The first simulation (Run 1, Table 3) had no addition of deep nitrate, and the sinking rate of detritus D was set to 0 (i.e. a closed system with no losses from the model domain). Results (at midnight each day) for the surface mixed layer are plotted in Fig. 2 (upper and bottom panels). The upper panel shows a small short-lived spring pulse up to about 0.5 mmol N m^{-3} in P, but otherwise mostly a constant value of about 0.3 (corresponding to a Chlorophyll α concentration of 0.4 mg m^{-3} for the conversion factor derived in the previous section). During summer both Z and D increase well above the P concentrations. N decreases by about 10% during the

Table 3
Parameter values for selected model simulations and average fluxes and f^* for the third year of the simulations (Units are the same for columns 5–9.)

Run	w_s ($m\,d^{-1}$)	r_e (d^{-1})	L_{Fe}	f_{up}	PP_{0-50} ($mol\,N\,m^{-2}\,yr^{-1}$)	f_{nm}	XP_{50}	XP_{120}	f^*
1	0	0.1	1.0	0	1.84	0.20	0.0	0.0	0.11
2	1	0.1	1.0	0	1.96	0.28	− 0.09	− 0.01	0.14
3	3	0.1	1.0	0.07	2.17	0.54	− 0.36	− 0.07	0.25
4	6	0.1	1.0	0.25	2.34	0.81	− 0.63	− 0.26	0.34
5	10	0.1	1.0	0.48	2.33	0.97	− 0.81	− 0.49	0.42
6	6	0.1	0.5	0.25	1.80	0.66	− 0.53	− 0.23	0.37
7	6	0.1	0.35	0.20	1.45	0.56	− 0.45	− 0.21	0.39
8	6	0.1	0.1	0.20	0.60	0.28	− 0.27	− 0.14	0.47
9	6	0.06	1.0	0.48	2.24	0.92	− 0.76	− 0.45	0.41
10	3	0.03	1.0	0.48	1.95	0.79	− 0.65	− 0.37	0.40
11	6	0.06	1.0	0.30	2.04	0.87	− 0.71	− 0.43	0.43
12	6	0.06	0.3	0.30	1.29	0.59	− 0.51	− 0.33	0.46
13	6	0.06	0.1	0.30	0.60	0.34	− 0.33	− 0.23	0.56

PP_{0-50} is set equal to f_{np} in Fig. 1.

summer, unlike observations that the summer surface nitrate concentrations are roughly half the winter values (Frost, 1993; Whitney and Freeland, 1999). The bottom panel shows the sea surface temperature, the mixed-layer depth (calculated as the depth at which the scalar turbulent mixing coefficient drops below $10^{-6}\,m^2\,s^{-1}$) and the depth of the 1% I_{PAR} level (taken to be the bottom of the euphotic zone). The mixed-layer depth shallows to about 15 m in summer and penetrates to the base of the model at 120 m in late winter. This shallow summer mixed-layer corresponds with several diagnoses of mixed layer depth from the observations (e.g. Martin, 1985; Archer et al., 1993; McClain et al., 1996); the range of annual sea surface temperature is also in agreement with the observations. The annual range for the 1% I_{PAR} depth corresponds with estimates in Welschmeyer et al. (1993) and Boyd et al. (1995a), but the detrital concentrations are high in this simulation because there are no losses due to sinking.

The second simulation, shown in the middle panel of Fig. 2, demonstrates the fundamental change in model behavior when the detritus is allowed to sink, in this case at a speed of $10\,m\,d^{-1}$. Without any means of nutrient replacement through advection, N concentrations decrease rapidly so that by the second summer, concentrations become limiting to phytoplankton growth and phytoplankton concentrations decrease to about $0.1\,mmol\,N\,m^{-3}$. In the third summer, P and consequently Z concentrations drop so low that when autumn mixing entrains N from between the seasonal mixed layer and 120 m into the mixed layer, the phytoplankton bloom because the Z concentrations are too low to control the phytoplankton production by grazing.

To demonstrate the dependence of nitrogen loss on sinking speed, we present in Fig. 3 a series of 5 yr simulations with detrital sinking speed w_s increasing from 3 to

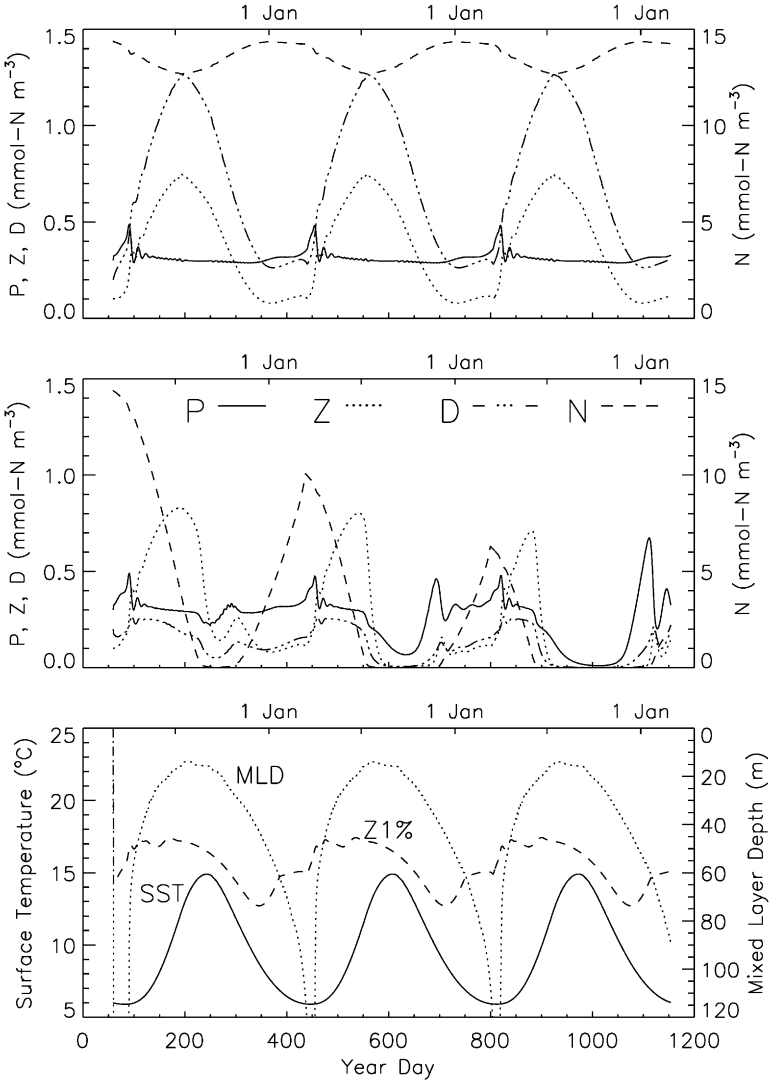

Fig. 2. Simulated upper layer 3-yr time series of P, Z, D and N (right-hand scale) with detritus sinking speeds of 0 (top panel – Run 1, Table 3) and 10 m d^{-1} (middle panel) with no Fe limitation and no deep nitrate addition. The bottom panel shows mixed-layer temperature (SST), mixed-layer depth (MLD) and 1% I_{PAR} penetration depth (Z1%) for Run 1. All values are at midnight.

10 m d^{-1}. For w_s equal to 3 m d^{-1} (top panel), there is a slow decreasing trend in the annual N cycle, with summer N likely to approach zero by about year 10. For w_s equal to 6 m d^{-1} (middle panel), the last (fifth) year resembles the third year when w_s equals 10 m d^{-1} (bottom panel), indicating that N becomes exhausted earlier as the detrital sinking speed increases. In the bottom panel, there apparently is just enough nutrient

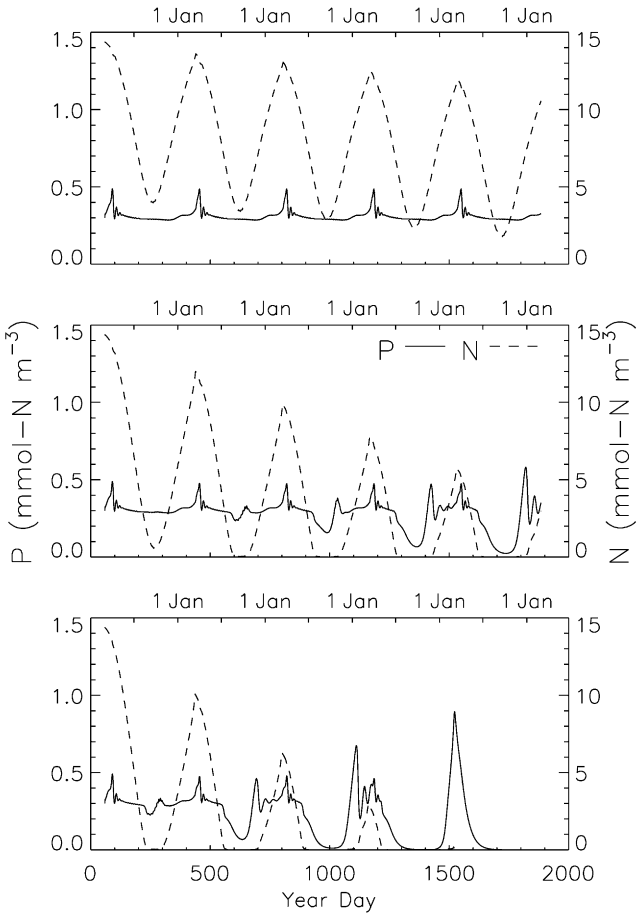

Fig. 3. Simulated 5-yr time series of upper layer P and N for detritus sinking speeds w_s of 3 (top), 6 (middle) and 10 m d^{-1} (bottom) with no Fe limitation and no deep nitrate addition.

for one large spring bloom (just after day 1500) after which there is insufficient N to support any significant phytoplankton biomass. Clearly, these simulations demonstrate that without a mechanism for addition of new nutrient to the model domain, the simulations with sinking detritus do not resemble observations at OSP: roughly constant P in the upper 50 m (Frost, 1993; Wong et al., 1995), and an annual cycle of surface nitrate ranging from ~ 8 to ~ 15 mmol N m^{-3} (Whitney and Freeland, 1999).

The annual heat and salt budgets in the upper ocean at OSP cannot be closed, i.e. net surface exchanges over 1 yr do not match the change in water column content over 1 yr (e.g., Large et al., 1994), indicating that horizontal transports are significant. Similarly, Archer et al. (1993) and Whitney and Freeland (1999) calculate that phosphate and nitrate are advected horizontally into the OSP region. In the next set

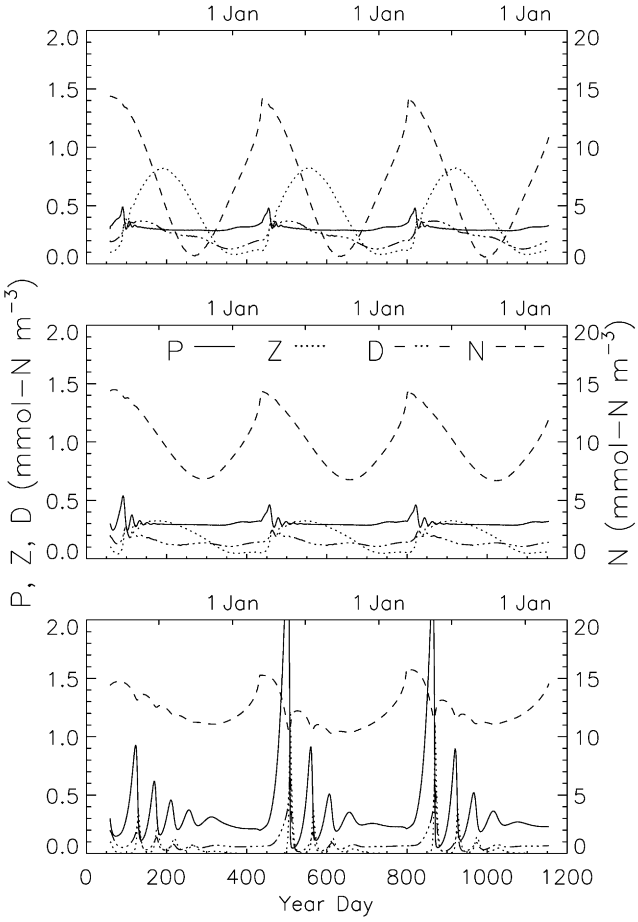

Fig. 4. Simulated upper layer 3-yr time series (Runs 4, 7 and 8) for Fe limitation $L_{Fe} = 1$ (no limitation, top panel), 0.35 (optimal limitation, middle panel), and 0.1 (extreme limitation, bottom panel).

of simulations, we introduced in each simulation a flux (constant in time) of nitrate into the N compartment, added over the bottom five layers in a manner that does not introduce a gradient at the bottom (since MY2.5 minimizes the vertical gradient at the bottom when the no-flux bottom boundary condition is applied). The amount of nitrate added was varied between 0.07 and 0.48 mol N m^{-3} yr^{-1}, sufficient to maintain nitrate-replete conditions in each simulation.

The surface layer values for simulations with the nitrogen addition and a sinking rate w_s of 6 m d^{-1} are presented in Fig. 4. The Fe limitation factor L_{Fe} takes on the values 1 (no limitation), 0.35 and 0.1, respectively, selected to demonstrate the three modes of behavior. The upper panel ($L_{Fe} = 1$) represents the same parameter set as the middle panel in Fig. 3, except for the nitrogen addition at depth. The phytoplankton

biomass P is basically flat except for a small increase each spring. The nitrogen pool N, although slowly declining, remains above the limiting values, but even in the first year drops to less than 10% of the winter value, rather than about 50% as observed. As L_{Fe} is reduced from 1, the maximum possible P growth rate (Eq. (6a)) is reduced accordingly. The middle panel shows the situation when the summer P growth rate has been reduced such that Z and D are both reduced, especially in summer, but surface layer N now cycles between about 15 and 7 mmol N m^{-3}, consistent with observations. Despite the zooplankton concentrations being suppressed somewhat, they are apparently maintained over winter at sufficient concentrations to control the spring increase in primary production such that only the small transitory increase in P occurs (Frost, 1993; Fasham, 1995). If we limit maximum P growth rate to 10% v_m ($L_{Fe} = 0.1$, bottom panel), we now reduce primary production in winter as well, causing the winter zooplankton concentrations to drop so low that a large spring bloom in P occurs because there are insufficient zooplankton to control the P concentration through grazing. We consider that the second simulation in Fig. 4, with an Fe limitation factor $L_{Fe} = 0.35$, best represents long-term observations of both surface layer P and N at OSP. In the next section, we analyze this model run in detail and consider its consistency with other observations.

5. Analysis and discussion

5.1. Vertical profiles

An advantage of a vertically resolved model is that variables and processes with significant vertical gradients, in and below the mixed layer, can be investigated in greater detail. In Fig. 5 we present depth–time sections for year 3 of Run 7, the simulation with the Fe limitation factor $L_{Fe} = 0.35$, for which surface layer values were plotted in the middle panel of Fig. 4.

The top panel of Fig. 5a shows the midnight mixed-layer depth and the depth of 1% surface I_{PAR} plotted over the temperature contours. The 1% light depth ranges between 60 and 80 m, consistent with most observations of Welschmeyer et al. (1993) and Varela and Harrison (1999). Other runs without Fe limitation that result in greater concentrations of detritus give 1% light depths as shallow as 40 m (e.g. Fig. 2), consistent with the shallowest observed depths. The middle panel shows the mean concentrations (0–50 m) for N, P, Z and D, similar to the surface values shown in Fig. 4, again showing that the Fe limitation at this level suppresses the concentrations of Z and D, but not P.

The bottom panel of Fig. 5a shows the depth structure for nitrogen, comprised mostly of nitrate. We can compare this panel with the top 120 m of the historical record of nitrate concentrations at OSP, shown in Fig. 2 of Matear (1995). The maximum gradient just below the mixed layer (September–October) from the model output is ~ 0.2 μM N m^{-1} ($=$ mmol N m^{-4}) and from the observations (~ 8 μM N/50 m $=$) ~ 0.15 μM N m^{-1}, but the contours of the observations will tend to smooth out and reduce the gradient because the observations are pooled from

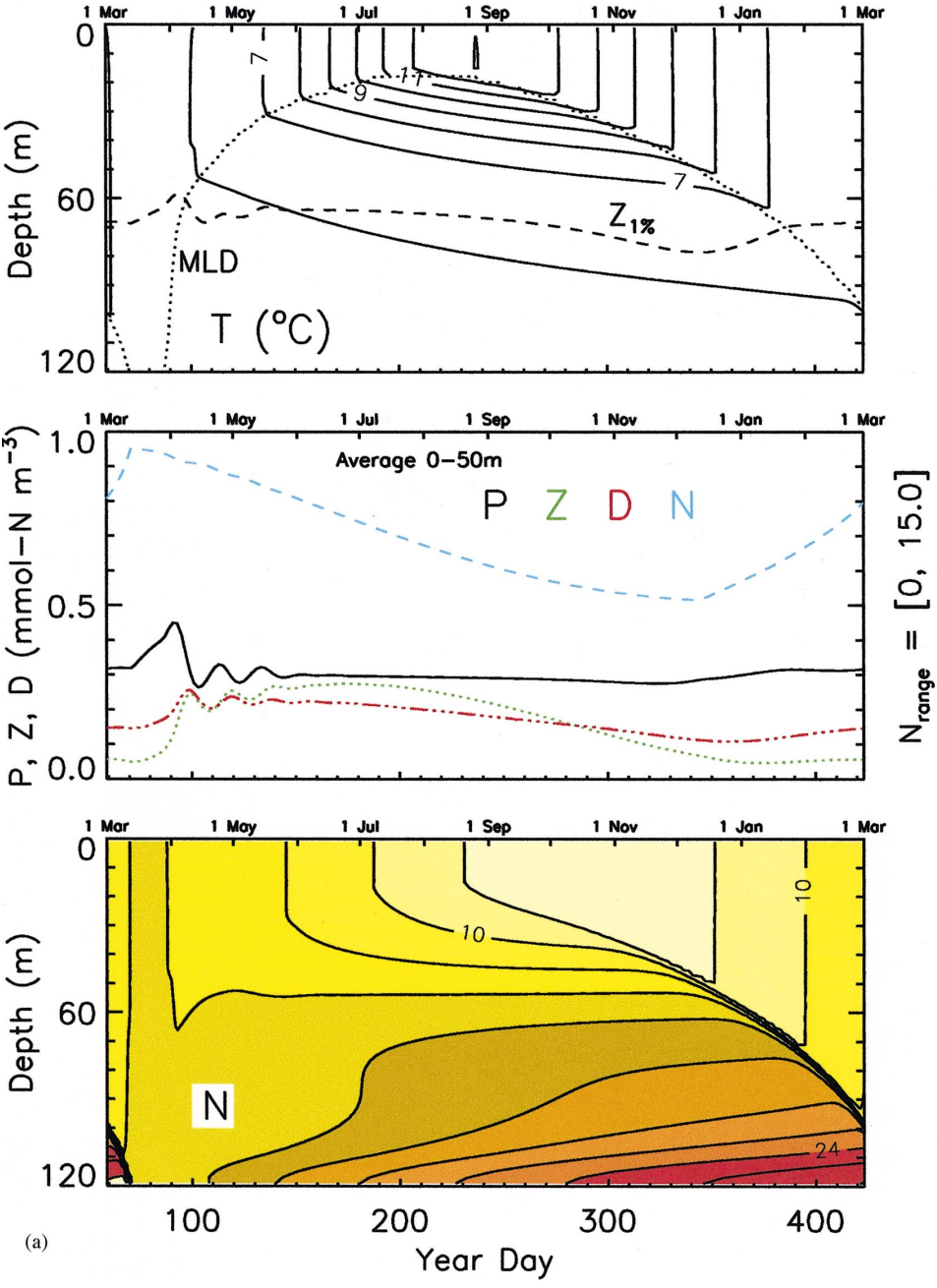

Fig. 5. Time–depth plots for year 3 of the Fe limitation simulation, Run 7. (a) Top panel: dotted line represents diagnosed mixed-layer depth and dashed line represents 1% I_{PAR} penetration depth. Middle panel: lines represent averages of P, Z, N and D over the depth range 0–50 m. Bottom panel: N contours in units of mmol N m^{-3}. (b) P (top), Z (middle) and D (bottom) contours in units of mmol N m^{-3}.

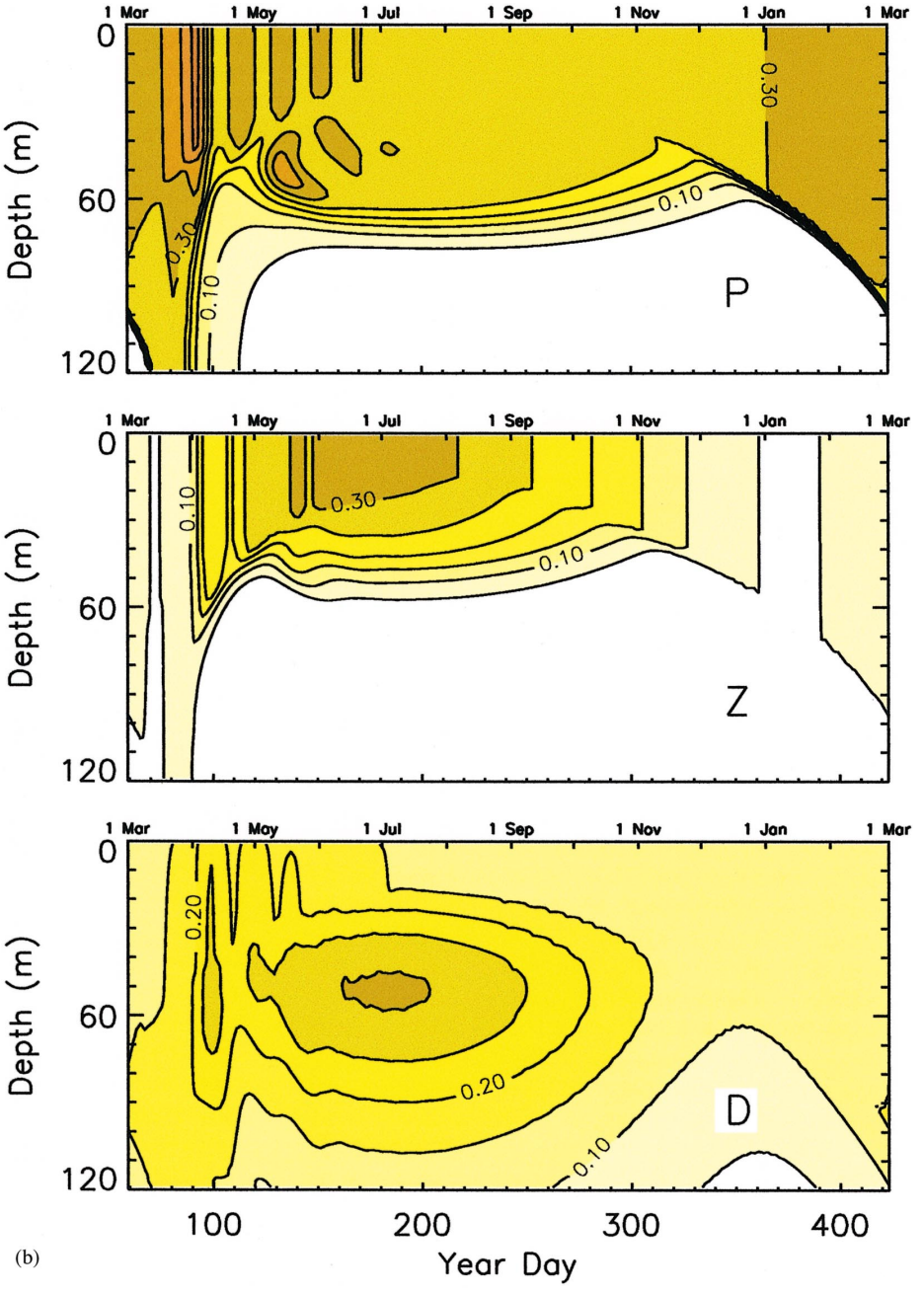

Fig. 5. Continued.

many years to generate a mean annual cycle. Also the contours in Matear (1995) are not continuous across 1 January. In January the 15 μM N contour probably should extend deeper, in which case the patterns above 10 m are comparable. In the modelled annual cycle, the upward diffusion of high nitrate from the addition over the bottom 10 m, and its subsequent entrainment over the whole water column upon the winter descent of the mixed layer to 120 m, is clear.

Fig. 5b shows the depth–time patterns for P, Z and D. Several points arise from the top panel showing P. First, there are $\sim$ 20-day oscillations in phytoplankton biomass in the mixed layer following the spring mixed layer shoaling (also evident in the middle panel of Fig. 5a). We believe that these small oscillations indicate limit cycle behavior following an initial increase in phytoplankton growth caused by the rapidly increasing irradiance and transient shallow daytime stratification (e.g., Woods and Barkmann, 1986; Zahariev, 1998). Popova et al. (1997) observed similar behavior in an NPZD model. Second, Fig. 5b demonstrates the importance, at least to the concentrations of P, Z and D, of the fraction of primary production, zooplankton grazing and growth, and detrital formation and remineralization that occurs below the mixed layer during most of the year (April–December). The peak in detritus occurs around 50 m, below most of its formation. At depths greater than 50 m, little detrital formation occurs and losses through remineralization occur as the detritus sinks towards the base of the model.

In our model, Z represents microzooplankton, which account for most of the grazing on the predominately small phytoplankton (Booth et al., 1993; Thibault et al., 1999). Booth et al. (1993) estimated concentrations of microzooplankton in the surface layer during May–September of 10–30 (mean $\sim$ 15) mg C m^{-3}, and Boyd et al. (1995b) obtained estimates over 80 m ($n = 2$) about $\frac{2}{3}$ those of Booth et al. With a Redfield conversion, the Booth et al. values indicate summer concentrations of 0.1–0.4 (mean 0.25) mmol N m^{-3}, comparable with concentrations in Figs. 4b, 5b and 6 (upper left), all for the Fe limitation simulation Run 7. In contrast, the summer microzooplankton concentrations in the Fe-replete simulation (Run 4, Fig. 4a) are twice the observed concentrations.

In Fig. 6, we present vertical profiles for the summer (22 June, top panels) and winter (21 December) solstices. In June more P and D biomass (and comparable Z biomass) is present below the mixed layer ($\sim$ 20 m) than within it. The P profile is roughly constant to almost 60 m, indicating that the model equations are near equilibrium (Denman et al., 1998), where P is a function of Z parameter values, which are constant with depth, and Z is a function of net production rate, which decreases with depth as I_{PAR} decreases. In December the subsurface maximum in D has disappeared and the mixed layer is deepening, but the buildup of deep N over the summer has yet to be entrained into the surface layer. These two figures demonstrate the advantage of a depth-resolved model, particularly in summer, over slab models where the mixed layer and the euphotic layer are not differentiated. Welschmeyer et al. (1993) and Boyd and Harrison (1999) both document significant primary production below the mixed layer throughout the spring–summer period, not unlike that displayed in the biomass concentrations shown in Figs. 5 and 6.

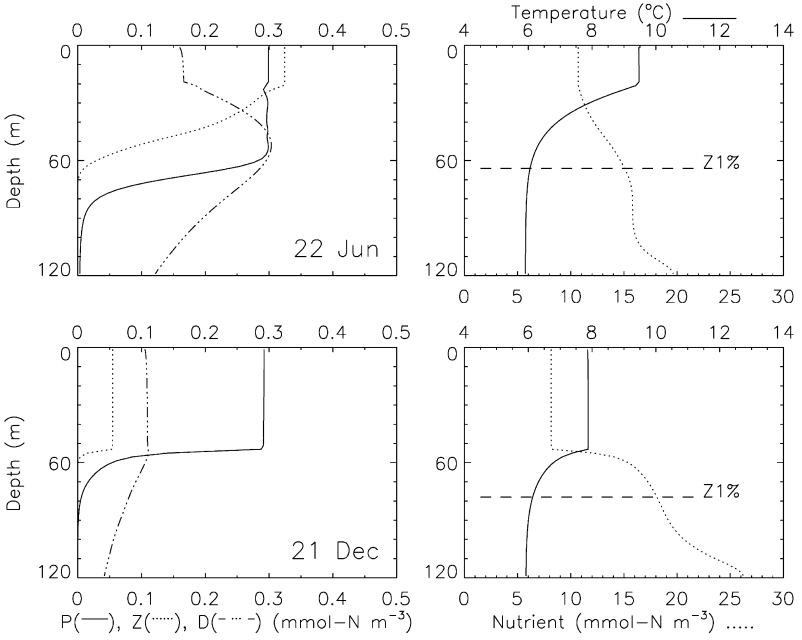

Fig. 6. Vertical profiles for Run 7, Year 3 at the summer (22 June, top panels) and winter (21 December, bottom panels) solstices.

5.2. Fluxes and f-ratios

The time and depth changes in the model simulations so far presented do not allow comparison with observed rate measurements – primary production rates, nitrogen uptake rates, sinking particle fluxes, etc. In Fig. 7 we present annual fluxes (in mol N m^{-2} yr^{-1}) corresponding to those shown in Fig. 1 for the Fe limitation simulation of Figs. 4–6 (Run 7). Fluxes between compartments are averaged over 0–50 m, and vertical fluxes are positive upwards. The fluxes of mixing across the 50-m level (double-ended arrows) represent primarily mixing associated with the annual cycle of the mixed layer rather than small-scale turbulent diffusion during the summer. Thus, net negative fluxes of P and Z represent downward entrainment of surface layer concentrations during early winter deepening of the mixed-layer past a depth of 50 m, and net positive fluxes of N and D represent upward fluxes from below 50 m during the same period. In Table 3 we present selected parameter values and annual fluxes for a subset of all simulations carried out in this study.

The flux f_{np}, from N to P, representing primary production, is 1.45 mol N m^{-2} yr^{-1} for the simulation described by Fig. 7 ($PP_{0\text{-}50}$, Run 7 in Table 3). Estimates from recent observations of carbon uptake (converted from C to N with the Redfield value of 6.6) are slightly higher: 2.1 (Welschmeyer et al., 1993) and 1.8 mol N m^{-2} yr^{-1} (Wong et al., 1995). Estimates of annual primary production from recent models of the

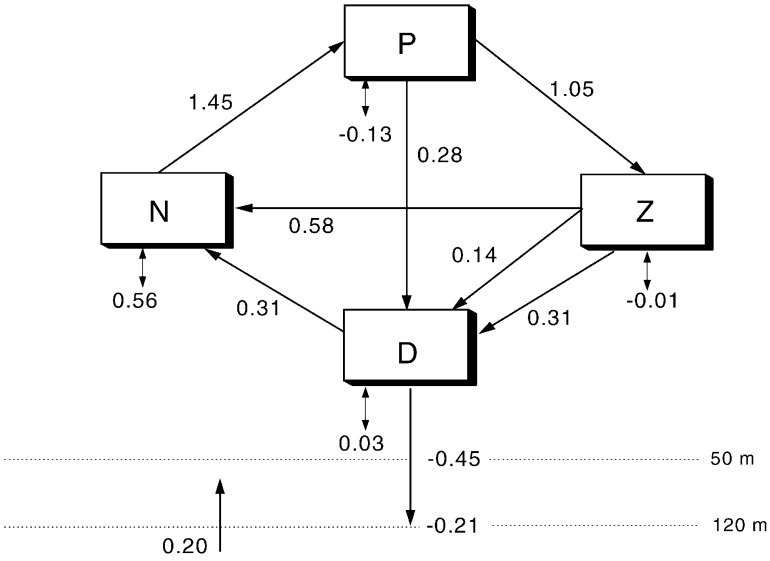

Fig. 7. Annual fluxes (in mol N m^{-2}) integrated over 0–50 m (Year 3, Run 7). Mixing fluxes across the 50-m level (double ended arrows) and sinking fluxes are positive upwards.

subarctic Pacific are even higher than observations: 2.9 (Frost, 1993), 2.0 (Fasham, 1995) and 2.4 mol N m^{-2} yr^{-1} (McClain et al., 1996). The export flux at 120 m, XP_{120} for Run 7 is 0.21 mol N m^{-2} yr^{-1}, compared with an estimate of 0.29 from three deployments of floating traps by Wong and Whitney (see Table 2). Studies employing ^{234}Th sorption typically give lower estimates of sinking fluxes than traps, but there is a discrepancy of a factor of 2 between conversion ratios for POC : ^{234}Th depending on whether trap material or suspended particles are analyzed (e.g. Charette et al., 1999; Quay, 1997). Emerson et al. (1991) estimated annual net biological O_2 production at OSP during 1987–1988 to be 2.8–4.2 mol O m^{-2} yr^{-1}. Converting to nitrogen using their $\Delta O/\Delta N$ ratio (determined from respiration-induced changes in the depth range 100–600 m) gives a range for export nitrogen flux of 0.29–0.43 mol N m^{-2} yr^{-1}. Given that the euphotic zone averages $\sim$ 70–80 m at OSP, this range should be compared with a modelled value between $XP_{50} = 0.45$ and $XP_{120} =$ 0.21 mol N m^{-2} yr^{-1} (for Run 7 in Table 3).

Other simulations documented in Table 3 resulted in higher primary production and export production. In particular, Run 6, with a less severe Fe limitation factor of $L_{Fe} = 0.5$, yielded larger values for annual primary production (1.8 mol N m^{-2} yr^{-1}) and annual export production at 120 m (0.23 mol N m^{-2} yr^{-1}) closer to estimates from flux observations. However, Run 6 gave a summer drawdown of surface nitrates of $\sim$ 10 mmol N m^{-3}, larger than the observed value of 7–8.

An apparent advantage of models that separate pools of new inorganic nitrogen (nitrate) from regenerated nitrogen (ammonium + urea) is that they can yield an *f*-ratio, the fraction of primary production (or nitrogen uptake) that is supported by

new, rather than regenerated, nitrogen. However, many studies (e.g., Dortch, 1990; Wheeler and Kokkinakis, 1990; Varela and Harrison, 1999) indicate that phytoplankton use regenerated forms of nitrogen preferentially. Under the assumption that phytoplankton will utilize first the available ammonium and urea and then utilize nitrate, we calculate a daily *f*-ratio (f^*) by taking ratios of the daily fluxes of nitrogen entering and leaving the N compartment:

$$f^* = \frac{f_{np} - (f_{zn} + f_{dn})}{f_{np}}, \tag{7}$$

where f_{np} represents the flux from N to P, etc. An annual mean *f*-ratio calculated from the annual fluxes with Eq. (7) is equivalent to the annual mean *f*-ratio obtained with models that distinguish between nitrate and ammonium pools.

The annual mean *f*-ratio, calculated for the top 50 m in our model, ranges between 0.11 and 0.56 (Table 3). Run 1, the initial reference run, has a detritus sinking speed of zero, but the annual cycle of the mixed layer across the 50-m level results in a small transport of N upwards across 50 m, and a small net transport of $(P + Z + D)$ downwards across 50 m, giving an annual mean *f*-ratio of 0.11. Runs 1–5 show that as the detritus sinking speed increases, the annual *f*-ratio also increases. The series of simulations with increasing Fe limitation (Runs 4, 6–8) result in increasing *f*-ratio, by reducing the fluxes to Z and D, and ultimately the recycling fluxes back to N. For Run 7, the simulation analyzed in detail in Figs. 5–7 with an annual *f*-ratio of 0.39, the daily primary production, daily grazing rate, f^*, and recycling and export fluxes are shown in Fig. 8. In the upper panel the daily integrated primary production (0–50 m) ranges between 2 and 6 mmol N m^{-2} d^{-1}. Recent observations of 24-h water column integrated C uptake can be converted as above giving values of 8.9 (June–August, 4 cruises, Welschmeyer et al., 1993), 2.5 (March 1993, Boyd et al., 1995b), 2.2 (February 1994, Boyd and Harrison, 1999) and 4.4 mmol N m^{-2} d^{-1} (May 1994, Boyd and Harrison). Other simulations with less Fe limitation (Table 3) resulted in higher annual and daily (not shown) rates of primary production.

The annual cycle of daily values of f^* are shown in the upper panel of Fig. 8. During periods of high regeneration and buildup of ammonium, daily f^* could become negative. However, for most of our simulations, this did not happen, indicating that for each day regenerated forms of nitrogen were insufficient to support all the nitrogen requirement. This high turnover rate for regenerated nitrogen is consistent with estimates of turnover time for ammonium at OSP of $\sim$ 1–3 days (Wheeler and Kokkinakis, 1990). The upper panel of Fig. 8 can be compared with Fig. 7c in Fasham (1995).

Except for one simulation, our model yields annual mean *f*-ratios smaller than the modelled estimate of 0.5 (Fasham, 1995) but in the range of the estimates in Fig. 12 from Frost (1993). From ^{15}N uptake experiments at OSP, Varela and Harrison (1999) estimated depth-integrated *f*-ratios that range 0.22–0.33 (mean 0.27, $n = 6$) for cruises spanning February to September, 1993–1994, and Wheeler and Kokkinakis (1990) estimated *f*-ratios that range 0.21–0.56 (mean 0.37, $n = 11$) for cruises spanning May to September, 1987–1988. Simultaneous measurements of depth-integrated nitrate

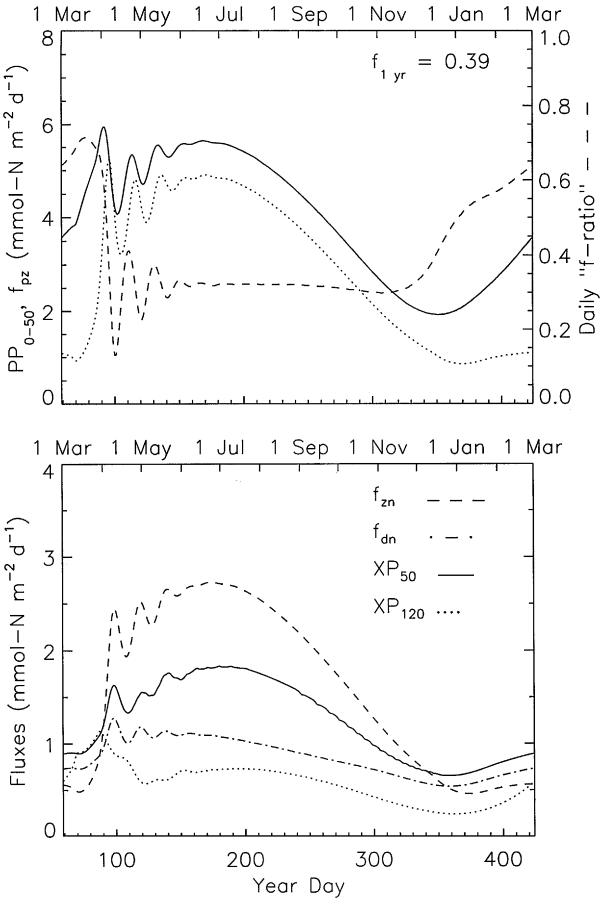

Fig. 8. Time series of selected daily mean fluxes for Run 7, Year 3. PP_{0-50} (solid line), the primary production over the top 50 m, is equivalent to the depth-integrated flux f_{np} in Fig. 1; f_{pz} (dotted line) is the depth-integrated phytoplankton loss flux to grazing. The daily "*f*-ratio" $f*$ is calculated according to Eq. (7). In the bottom panel, the daily mean recycling fluxes f_{zn} and f_{dn} are compared with the export fluxes.

uptake rate (Wheeler, 1993) and depth-integrated primary production (Welschmeyer et al., 1993) for the same four cruises to OSP result in means of 45 mg N m^{-2} d^{-1} and 707 mg C m^{-2} d^{-1}, respectively. Converting to the same units using the Redfield value of 6.6 (atom : atom), we obtain a value of 0.36 for mean *f*-ratio. The modelled annual mean *f*-ratio for the Fe limitation Run 7 of 0.39 is higher than the mean of 0.27 from Varela and Harrison, but comparable with the means from SUPER of 0.36 and 0.37. Run 3 did yield a lower value of 0.25 for annual mean *f*-ratio, but the remineralization depth scale (w_s/r_e) of 30 m is much smaller than the range 100–260 m, estimated from the vertical gradient in sinking fluxes (Table 2).

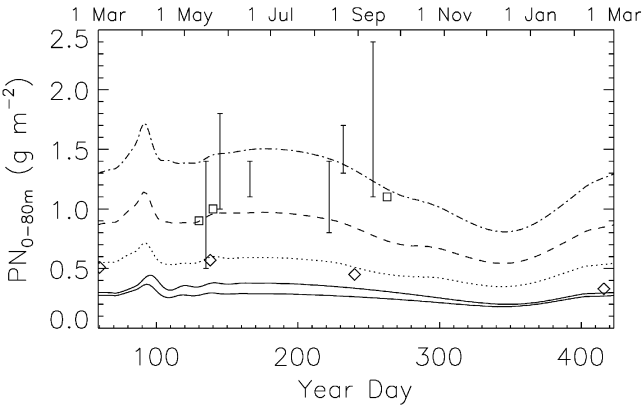

Fig. 9. Particulate nitrogen PN integrated over the depth range 0–80 m (in g N m^{-2}). The solid lines represent lower ($P + D$) and upper ($P + D + Z$) estimates of PN for the Fe limitation Run 12. The other lines represent ($P + D$) estimates of PN for Runs 5, 9 and 10 (increasing upwards with decreasing detritus sinking speeds 10, 6 and 3 m d^{-1}). All simulations had a remineralization length scale (w_s/r_e) of 100 m. Vertical bars represent ranges of PN measurements (for 6 cruises) from Wheeler (1993), squares represent estimates over the euphotic zone (for 3 cruises) from Varela and Harrison (1999), and diamonds represent estimates from transmissometer-derived POC converted from C to N by the C : N ratio in (1–53 μm) samples collected with large volume pumps (J. Bishop, pers. comm.). A grand average from Niskin bottles for 6 cruises during April–May 1988, 92, 93, 94, 95 and 96 was 0.84 g N m^{-2} (C.S. Wong and F. Whitney, pers. comm.).

The apparent increase in annual *f*-ratio with increased detritus sinking speeds (Runs 1–5, Table 3) may be confounded by the decrease in remineralization depth scale caused by holding the remineralization rate r_e constant at 0.1 d^{-1}. To investigate this effect, we consider Runs 5, 9 and 10, with sinking speeds 10, 6 and 3 m d^{-1} and compensating remineralization rates of 0.1, 0.06 and 0.03 d^{-1}, respectively (so as to maintain a constant remineralization depth scale of 100 m; see Table 2 and Charette et al., 1999). Although most annual mean fluxes varied significantly, all three simulations yielded an annual mean *f*-ratio of about 0.4, indicating that the remineralization length scale rather than the detritus sinking speed is more important in determining the *f*-ratio. On the other hand, increasing the remineralization time scale (decreasing r_e), while maintaining the remineralization depth scale constant, affects the model dynamics in the upper 50 m by increasing the concentrations of Z and D and introducing a greater delay in returning nitrogen to N from Z and D.

To demonstrate this sensitivity to r_e for a constant remineralization depth scale, we present in Fig. 9 the annual cycle in ($P + D$) for Runs 7, 9, 10 and 12, which can be compared with particulate nitrogen (PN) observations if the amount associated with microzooplankton is neglected (for Run 12, we also plot ($P + D + Z$) as an upper bound for PN). Run 12, an Fe-limitation simulation, results in low, roughly constant values of PN. As we reduce r_e and w_s (Runs 7, 9 and 10), the PN increases significantly. Wheeler (1993) has made the most complete observations of depth-integrated (0–80 m) PN at OSP (during the period May–September in three different years),

which range from 0.5 to 2.4 g N m^{-2}. Varela and Harrison (1999) observed similar PN concentrations in the euphotic zone of 0.9–1.1 g N m^{-2} during three cruises in the months of May (2) and September. These observations fall mostly in the range of the upper two curves in Fig. 9. Estimates of PN from beam transmission and water column filtration, provided by J. Bishop (pers. comm., based on observations in Bishop et al., 1999), range 0.3–0.6 g N m^{-2}, closer to the modelled curves of Run 12.

Because a longer remineralization time scale might seem to favor higher PN concentrations, we reran the Fe-limitation simulations, but with r_e equal to 0.06 rather than 0.1 d^{-1}, in Runs 11–13. In this series, a surface-layer nitrate drawdown to about 7–8 mmol N m^{-3} (Run 12) occurred at a slightly lower value (stronger Fe limitation) of 0.3 for L_{Fe} compared with 0.35 in Run 7. However, the time series for P, Z, N and D were essentially unchanged from those plotted in Fig. 4. Because of the deeper remineralization, the annual mean f-ratios in Runs 11–13 were greater than those in Runs 5, 7 and 8, a change apparently in the wrong direction relative to observations.

5.3. Reconciliation with observations

Selection of parameter values (or ranges) is crucial to the behavior and outcome of model simulations. However, even with parameter estimation or data assimilation procedures (e.g., Fasham and Evans, 1995; Matear, 1995; Hurtt and Armstrong, 1996), the setting of acceptable ranges for parameters which do not correspond directly to quantities derived from observations is largely arbitrary. We have attempted to constrain the model parameter values (and hence results) with observations. The Fe-limitation simulations were evaluated according to the ability to approach simultaneously the observed long-term annual cycles of upper layer phytoplankton biomass and nitrate concentrations. They also produce microzooplankton concentrations comparable with the limited observations. However, the "best" simulations (Runs 7 and 12) yielded an annual f-ratio larger than that of Varela and Harrison (1999) but comparable with estimates from SUPER, PN concentrations lower than observations, and a remineralization length scale less than that derived from gradients of sinking fluxes measured with drifting sediment traps (Wong and Whitney, pers. comm.). These deviations from observations were of order $\sim 50\%$, probably within the range of observational uncertainty and/or seasonal and interannual variability. Most adjustments to the model to increase PN and maintain a reasonably large remineralization depth scale increase the annual mean f-ratio further, but still to values generally less than f-ratios obtained in earlier models of OSP.

We do not believe that increasing the number of compartments or subjecting the model to a parameter optimization technique will necessarily improve reconciliation with observations. Fasham (1995), with a seven-compartment model, obtained an annual f-ratio of 0.5, which now appears to be too high. Matear (1995), using a simulated annealing optimization technique, found it necessary to constrain the f-ratio in an optimization of the seven-component model of Fasham et al. (1990). Otherwise Matear's optimization produced an f-ratio that varied during the year over

the range 0.8–1.0. Recent observations of Kirchman and Wheeler (1998) from the subarctic Pacific show that heterotrophic bacteria account for roughly one-third of the total uptake of nitrate and ammonium, suggesting that the estimation of *f*-ratios from nitrogen uptake measurements may need revision.

An emerging paradigm for controlling factors in HNLC regimes (e.g. Cullen, 1995; Landry et al., 1997) includes the control of picoplanktonic biomass by microzooplanktonic grazing and the control of diatom biomass by scarcity of Fe limiting their growth rate. Concerning grazing, we chose the formulation and parameter values representing grazing by microzooplankton such that the grazing losses by the phytoplankton community should be comparable with the growth rates of the phytoplankton at OSP. In the top panel of Fig. 8, the grazing losses f_{pz} track the primary production rate PP_{0-50} with little time lag at 0.6–0.8 of PP_{0-50} between 1 April and 1 December, consistent with observations of Landry et al. (1993) and Boyd et al. (1995b,1996). During the winter months, neither Fe nor grazing limitation are required because the phytoplankton are generally light limited, consistent with the observations of Boyd et al. (1995b) and Maldonado et al. (1999). However, in both the model and at OSP, the microzooplankton remain capable of controlling any rapid increase in phytoplankton biomass (Boyd et al., 1995b). Concerning limitation by Fe, in our model the optimal simulations of Fe limitation occurred when the maximum attainable phytoplankton growth rate was reduced by a factor $L_{Fe} = 0.3$–0.35. Does this mean that the primary production would increase threefold if Fe limitation were removed, and is there evidence for a factor of three? Because L_{Fe} would be the limiting factor only when the light limitation factor is greater than L_{Fe} (i.e. less light limitation), the realized increase would be less if Fe limitation were removed. From Table 3, the ratio of annual primary production without Fe limitation to that with Fe limitation (Runs 4–7, and 9–12) is ~ 1.7, not 3. From several-day Fe enrichment experiments, Boyd et al. (1996) estimated algal growth rates in Fe-enriched carboys to be roughly twice those in control carboys. However, we do not want to attach too much significance to the exact values of L_{Fe}, etc., because of the simplicity of the model.

What modifications to our model might lead to better reconciliation of model results with observations at OSP? It seems that more particulate nitrogen must remain in the euphotic zone (suggesting a small remineralization length scale), but sinking detritus at depths of 100–200 m, below the euphotic zone, must retain a remineralization length scale of at least 100 m. We plan three possible changes. First, the remineralization length scale (w_s/r_e) could increase with depth, as suggested by sediment flux observations. Second, the detrital compartment could be divided into one compartment representing dissolved organic matter and non-sinking particles and one compartment representing sinking organic particles such as mesozooplankton fecal particles. Then, the remineralization length scale of the sinking particles could be adjusted independently from that of the non-sinking organic matter. Third, if winter estimates of autotrophic C : Chl (and N : Chl) ratios can be obtained for OSP to calibrate C : Chl models (e.g., Geider et al., 1997; Taylor et al., 1997), then chlorophyll could be modelled as a separate variable, such that the rate of primary production of C (or uptake of N) could be dependent on modelled chlorophyll

biomass (e.g. Doney et al., 1996), in closer accordance with observations. However, as Matear (1995) concluded, successful optimization of a more complex model requires additional measurements to constrain the added fluxes and compartment pool sizes.

It may be that the ecological model is not inadequate at all. Archer et al. (1993) concluded that horizontal advection of salt and macronutrients contributes significantly to the local balance at OSP, and Large et al. (1994) applied advection of heat and salt at OSP in their mixed-layer simulations of the annual cycle. If there were horizontal advection of nitrate to the surface layer at OSP during the growing season, then a weaker Fe limitation would be required to limit the summer drawdown of surface nitrate to the long-term observed value of $\sim$ 7–8 mmol N m^{-3}.

Finally, different model structures may be employed to probe different aspects of marine ecosystems. Vézina and Savenkoff (1999) have used an inverse model to analyze the foodweb structure and dynamics at OSP during three cruise periods – in winter, spring and late summer. They conclude that despite relative uniformity over the season in extensive variables representing physical, chemical and biological fields and the export fluxes of C and N at 200 m, the foodweb structure changes dramatically with season. In common with our work, they emphasize the importance of the detrital pool, and they conclude that during spring the foodweb is not in steady state, suggesting predator–prey oscillations.

6. Summary

We have simulated a simple Fe control on phytoplankton at OSP with a coupled 1-d mixed layer/four-compartment ecosystem model. Although there is only one nitrogen compartment, the annual *f*-ratio can be calculated by modifying the standard formula to use the recycled nitrogen entering the nitrogen compartment. The Fe-limitation factor, constant during the year, was reduced from 1.0 (no limitation of maximum phytoplankton growth rate) in steps down to 0.1 (limitation of maximum phytoplankton growth rate to 10% of the maximum possible rate for saturating amounts of nitrogen and I_{PAR}). The most likely level (0.3–0.35) was taken as that level where the summer drawdown of surface nitrate agreed with the long-term observed value of 7–8 mmol N m^{-3}. Those simulations, when compared with observations, resulted in an annual *f*-ratio that is high, primary production and particulate nitrogen concentrations that are low, and a remineralization length scale that may be too small. We caution against trying to estimate an annual cycle from observations taken in different years. Wong (1989), Wong et al. (1995,1999) demonstrate that annual rates of primary production (measured with the same techniques) and of particle sedimentation both vary by at least a factor of two. Nevertheless, we feel that several extensions to our model should improve its simultaneous agreement with different types of observations: (i) increasing the particle sinking speed and/or decreasing the remineralization rate with depth; (ii) dividing the detritus compartment into (a) non-sinking particles and dissolved organic matter, and (b) sinking particles; and (iii) estimating possible horizontal fluxes of nitrate in the surface layer or embedding the model in an ocean general circulation model with horizontal advective terms.

Acknowledgements

We have benefitted from discussions especially with Geoff Evans, Mike Fasham, Bruce Frost, Alain Vézina, Patrick Cummins, and the participants of the JGOFS Modelling Workshop in Toulouse, France in 1995. We found the annual meetings and modelling workshops of Canadian JGOFS immensely valuable, and thank all the participants of the North Pacific study, especially David Mackas, Frank Whitney, Philip Boyd, Nelson Sherry, Paul Harrison and Claude Savenkoff. Our colleague Susan Haigh showed us how to solve the model for an analytic equilibrium solution. We thank three reviewers for thoughtful and constructive comments, and finally we thank Bruce Johnson for holding the project together.

References

Antoine, D., Morel, A., 1995a. Modelling the seasonal course of the upper ocean pCO_2 (I) Development of a one-dimensional model. Tellus 47B, 103–121.

Antoine, D., Morel, A., 1995b. Modelling the seasonal course of the upper ocean pCO_2 (II) Validation of the model and sensitivity studies. Tellus 47B, 122–144.

Archer, D., Emerson, S., Powell, T., Wong, C.S., 1993. Numerical hindcasting of sea surface pCO_2 at Weathership Station Papa. Progress in Oceanography 32, 319–351.

Bacon, M.P., Cochran, J.K., Hirschberg, D., Hammar, T.R., Fleer, A.P., 1996. Export flux of carbon at the equator during the EqPac time-series cruises estimated from ^{234}Th measurements. Deep-Sea Research II 43, 1133–1153.

Banse, K., 1991. Iron availability, nitrate uptake, and exportable new production in the subarctic Pacific. Journal of Geophysical Research 96, 741–748.

Bishop, J.K., 1999. Transmissometer measurement of POC. Deep-Sea Research I 46, 353–369.

Bishop, J.K.B., Calvert, S., Soon, M., 1999. Seasonal and temporal variability of POC in the northeast subarctic Pacific. Deep-Sea Research II 46, 2699–2733.

Booth, B.C., Lewin, J., Postel, J.R., 1993. Temporal variation in the structure of autotrophic and heterogrophic communities in the subarctic Pacific. Progress in Oceanography 32, 57–99.

Boyd, P.W., Harrison, P.J., 1999. Phytoplankton dynamics in the NE subarctic Pacific. Deep-Sea Research II 46, 2405–2432.

Boyd, P.W., Harrison, P.J., Johnson, B.D., 1999. JGOFS Canada studies in the NE subarctic Pacific – an overview. Deep-Sea Research II 46, 2345–2350.

Boyd, P.W., Muggli, D.L., Varela, D.E., Goldblatt, R.H., Chretien, R., Orians, K.J., Harrison, P.J., 1996. In vitro iron enrichment experiments in the NE subarctic Pacific. Marine Ecology Progress Series 136, 179–193.

Boyd, P.W., Strom, S., Whitney, F.A., Doherty, S., Wen, M.E., Harrison, P.J., Wong, C.S., 1995a. The NE Subarctic Pacific in Winter: I. Biological standing stocks. Marine Ecology Progress Series 128, 11–24.

Boyd, P.W., Whitney, F.A., Harrison, P.J., Wong, C.S., 1995b. The NE Subarctic Pacific In Winter: II. Biological rate processes. Marine Ecology Progress Series 128, 25–34.

Chai, F., Lindley, S.T., Barber, R.T., 1996. Origin and maintenance of a high nitrate condition in the equatorial Pacific. Deep-Sea Research II 43, 1031–1064.

Charette, M.A., Moran, S.B., Bishop, J.K.B., 1999. ^{234}Th as a tracer of particulate organic carbon export in the subarctic northeast Pacific Ocean. Deep-Sea Research II 46, 2833–2861.

Chisholm, S.W., Morel, F.M. (Eds.), 1991. What controls phytoplankton production in nutrient-rich areas of the open sea? Limnology and Oceanography 36, 1507–1970.

Clegg, S.L., Whitfield, M., 1990. A generalized model for the scavenging of trace metals in the open ocean – I. Particle cycling. Deep-Sea Research 37, 809–832.

Cullen, J.J., 1995. Status of the Iron hypothesis after the open-ocean enrichment experiment. Limnology and Oceanography 40, 1336–1343.

Cullen, J.J., Geider, R.J., Ishizaka, J., Kiefer, D.A., Marra, J., Sakshaug, E., Raven, J.A., 1993. Toward a general description of phytoplankton growth for biogeochemical models. In: Evans, G.T., Fasham, M.J.R. (Eds.), Towards a Model of Ocean Biogeochemical Processes. Springer, Berlin, pp. 153–176.

Davis, C.S., Steele, J.H. (Eds.), 1994. Biological/Physical Modeling of Upper Ocean Processes, Woods Hole Oceanographic Institution. Technical Report WHOI-94-32, 64 p.

Denman, K.L., 1973. A time-dependent model of the upper ocean. Journal of Physical Oceanography 3, 173–184.

Denman, K.L., Gargett, A.E., 1995. Biological–physical interactions in the upper ocean: the role of vertical and small scale transport processes. Annual Reviews of Fluid Mechanics 27, 225–255.

Denman, K.L., Miyake, M., 1973. Upper layer modification at Ocean Station Papa: observations and simulation. Journal of Physical Oceanography 3, 185–196.

Denman, K.L., Peña, M.A., Haigh, S.P., 1998. Simulations of marine ecosystem response to climate variation with a one dimensional coupled ecosystem/mixed layer model. In: Müller P., Holloway G. (Eds.), Biotic Impacts of Extratropical Climate Change in the Pacific. Proceedings 'Aha Huliko'a Hawaiian Winter Workshop, pp. 141–147.

Dobson, F.W., Smith, S.D., 1988. Bulk models of solar radiation at sea. Quarterly Journal of the Royal Meteorological Society 114, 165–182.

Doney, S.C., Glover, D.M., Najjar, R.G., 1996. A new coupled, one-dimensional biological–physical model for the upper ocean: applications to the JGOFS Bermuda Atlantic Time Series (BATS) site. Deep-Sea Research II 43, 591–624.

Dortch, Q., 1990. The interaction between ammonium and nitrate uptake in phytoplankton. Marine Ecology Progress Series 61, 183–201.

Dunne, J.P., Murray, J.W., Young, J., Balistrieri, L.S., Bishop, J., 1997. ^{234}Th and particle cycling in the central equatorial Pacific. Deep-Sea Research II 44, 2049–2083.

Emerson, S., Quay, P., Stump, C., Wilbur, D., Knox, M., 1991. O_2, Ar, N_2, and ^{222}Rn in surface waters of the subarctic ocean: net biological O_2 production. Global Biogeochemical Cycles 5, 49–69.

Evans, G., Garçon V. (Eds.), 1997. One-Dimensional Models of Water Column Biogeochemistry. JGOFS Report 23/97. JGOFS Bergen, Norway, 85 p.

Evans, G.T., Parslow, J.S., 1985. A model of annual plankton cycles. Biological Oceanography 3, 327–347.

Fasham, M.J.R., 1995. Variations in the seasonal cycle of biological production in subarctic oceans: a model sensitivity analysis. Deep-Sea Research I 42, 1111–1149.

Fasham, M.J.R., Ducklow, H.W., McKelvie, S.M., 1990. A nitrogen-gased model of plankton dynamics in the oceanic mixed layer. Journal of Marine Research 48, 591–639.

Fasham, M.J., Evans, G.T., 1995. The use of optimization techniques to model marine ecosystem dynamics at the JGOFS station at 47°N 20°W. Philosophical Transactions of the Royal Society of London B 348, 203–209.

Freeland, H., Denman, K., Wong, C.S., Whitney, F., Jacques, R., 1997. Evidence of change in the winter mixed layer in the Northeast Pacific Ocean. Deep-Sea Research I 44, 2117–2129.

Frost, B.W., 1987. Grazing control of phytoplankton stock in the open subarctic Pacific Ocean: a model assessing the role of mesozooplankton, particularly the large calanoid copepods. Marine Ecology Progress Series 39, 49–68.

Frost, B.W., 1993. A modelling study of processes regulating plankton standing stock and production in the open subarctic Pacific Ocean. Progress in Oceanography 32, 17–56.

Frost, B.W., Franzen, N.C., 1992. Grazing and iron limitation in the control of phytoplankton stock and nutrient concentration: a chemostat analogue of the Pacific equatorial upwelling zone. Marine Ecology Progress Series 83, 291–303.

Garçon, V.C., Thomas, F., Wong, C.S., Minster, J.-F., 1992. Gaining insight into the seasonal variability of CO_2 at Ocean Station P using an upper ocean model. Deep-Sea Research 39, 921–938.

Geider, R.J., MacIntyre, H.L., Kana, T.M., 1997. Dynamic model of phytoplankton growth and acclimation: responses of the balanced growth rate and the chlorophyll *a*: carbon ratio to light, nutrient-limitation and temperature. Marine Ecology Progress Series 148, 187–200.

Haney, J.D., Jackson, G.A., 1996. Modeling phytoplankton growth rates. Journal of Plankton Research 18, 63–85.

Harrison, W.G., Harris, L.R., Irwin, B.D., 1996. The kinetics of nitrogen utilization in the oceanic mixed layer: nitrate and ammonium interactions at nanomolar concentrations. Limnology and Oceanography 41, 16–32.

Hurtt, G.C., Armstrong, R.A., 1996. A pelagic ecosystem model calibrated with BATS data. Deep-Sea Research II 43, 653–683.

Iqbal, M., 1983. Introduction to Solar Radiation. Academic Press, Toronto, 390 p.

Johnson, K.S., Gordon, R.M., Coale, K.H., 1997. What controls dissolved iron concentrations in the world ocean? Marine Chemistry 57, 137-161.

Kantha, L.H., Clayson, C.A., 1994. An improved mixed layer model for geophysical applications. Journal of Geophysical Research 99, 25235–25266.

Kawamiya, M., Kishi, M.J., Yamanaka, Y., Suginohara, N., 1995. An ecological–physical coupled model applied to Station Papa. Journal of Oceanography 51, 635–664.

Kirchman, D.L., Wheeler, P.A., 1998. Uptake of ammonium and nitrate by heterotrophic bacteria and phytoplankton in the sub-Arctic Pacific. Deep-Sea Research I 45, 347–365.

Landry, M.R., Monger, B.C., Selph, K.E., 1993. Time-dependency of microzooplankton grazing and phytoplankton growth in the subarctic Pacific. Progress in Oceanography 32, 205–222.

Landry, M.R., Barber, R.T., Bidigare, R.R., Chai, F., Coale, K.H., Dam, H.G., Lewis, M.R., Lindley, S.T., McCarthy, J.J., Roman, M.R., Stoecker, D.K., Verity, P.G., White, J.R., 1997. Iron and grazing constraints on primary production in the central equatorial Pacific: An EqPac synthesis. Limnology and Oceanography 42, 405–418.

Large, W.G., McWilliams, J.C., Doney, S.C., 1994. Ocean vertical mixing: a review and a model with a nonlocal boundary layer parameterization. Reviews of Geophysics 32, 363–403.

Lean, J., 1991. Variations in the Sun's radiative output. Reviews of Geophysics 29, 505–535.

Loukos, H., Frost, B., Harrison, D.E., Murray, J.W., 1997. An ecosystem model with iron limitation of primary production in the equatorial Pacific at 140°W. Deep-Sea Research II 44, 2221–2249.

Maldonado, M.T., Boyd, P.W., Harrison, P.J., Price, N.M., 1999. Co-limitation of phytoplankton growth by light and Fe during winter in the NE subarctic Pacific Ocean. Deep-Sea Research II 46, 2475–2485.

Maldonado, M.T., Price, N.M., 1999. Utilization of iron bound to strong organic ligands by plankton communities in the subarctic Pacific Ocean. Deep-Sea Research II 46, 2447–2473.

Martin, J.H., Fitzwater, S.E., 1988. Iron deficiency limits phytoplankton growth in the northeast Pacific subractic. Nature 331, 341–343.

Martin, J.H., Gordon, R.M., 1988. Northeast Pacific iron distributions in relation to phytoplankton productivity. Deep-Sea Research 35, 177–196.

Martin, J.H., Gordon, R.M., Fitzwater, S., Broenkow, W.W., 1989. VERTEX: phytoplankton/iron studies in the Gulf of Alaska. Deep-Sea Research 36, 649–680.

Martin, P.J., 1985. Simulation of the mixed layer at OWS November and Papa with several models. Journal of Geophysical Research 90, 903–916.

Matear, R.J., 1995. Parameter optimization and analysis of ecosystem models using simulated annealing: A case study at Station P. Journal of Marine Research 53, 571–607.

Matear, R.J., Wong, C.S., 1997. Estimation of vertical mixing in the upper ocean at Station P from chlorofluorcarbons. Journal of Marine Research 55, 507–521.

McClain, C.R., Arrigo, K., Tai, K.-S., Turk, D., 1996. Observations and simulations of physical and biological processes at ocean weather station P, 1951–1980. Journal of Geophysical Research 101, 3697–3713.

McGillicuddy Jr., D.J., McCarthy, J.J., Robinson, A.R., 1995. Coupled physical and biological modeling of the spring bloom in the North Atlantic (I): model formulation and one dimensional bloom processes. Deep-Sea Research I 42, 1313–1357.

Mellor, G.L., Yamada, T., 1974. A hierarchy of turbulence closure models for planetary boundary layers. Journal of the Atmospheric Sciences 31, 1791–1806.

Mellor, G.L., Yamada, T., 1982. Development of a turbulent closure model for geophysical fluid problems. Reviews of Geophysics and Space Physics 20, 851–875.

Miller, C.B., Frost, B.W., Wheeler, P.A., Landry, M.R., Welschmeyer, N., Powell, T.M., 1991. Ecological dynamics in the subarctic Pacific, a possibly iron-limited ecosystem. Limnology and Oceanography 36, 1600–1615.

Morel, A., Smith, R.C., 1974. Relation between total quanta and total energy for aquatic photosynthesis. Limnology and Oceanography 19, 591–600.

Parsons, T.R., Lalli, C.M., 1988. Comparative oceanic ecology of the plankton communities of the subarctic Atlantic and Pacific Oceans. Oceanography and Marine Biology: an Annual Review 26, 51–68.

Popova, E.E., Fasham, M.J., Osipov, A.V., Ryabchenko, V.A., 1997. Chaotic behaviour of an ocean ecosystem model under seasonal external forcing. Journal of Plankton Research 19, 1495–1515.

Prunet, P., Minster, J.-F., Ruiz-Pino, D., Dadou, I., 1996a. Assimilation of surface data in a one-dimensional physical–biogeochemical model of the surface ocean 1. Method and preliminary results. Global Biogeochemical Cycles 10, 111–138.

Prunet, P., Minster, J.-F., Echevin, V., Dadou, I., 1996b. Assimilation of surface data in a one-dimensional physical–biogeochemical model of the surface ocean 2. Adjusting a simple trophic model to chlorophyll, temperature, nitrate, and pCO_2 data. Global Biogeochemical Cycles 10, 111–138.

Quay, P., 1997. Was a carbon balance measured in the equatorial Pacific during JGOFS? Deep-Sea Research II 44, 1765-1781.

Schmidt, M.A., Hutchins, D.A., 1999. Size-fractionated biological iron and carbon uptake along a coastal to offshore transect in the NE Pacific. Deep-Sea Research II 46, 2487–2503.

Spencer, J.W., 1971. Fourier series representation of the position of the sun. Search 2, 172.

Steele, J.H., Henderson, E.W., 1992. The role of predation in plankton models. Journal of Plankton Research 14, 157–172.

Sunda, W.G., Huntsman, S.A., 1997. Interrelated influence of iron, light and cell size on marine phytoplankton growth. Nature 390, 389–392.

Taylor, A.H., Geider, R.J., Gilbert, F.J., 1997. Seasonal and latitudinal dependencies of phytoplankton carbon-to-chlorophyll *a* ratios: results of a modelling study. Marine Ecology Progress Series 152, 51–66.

Thibault, D., Roy S., Wong C.S., 1999. The downward flux of biogenic material in the NE subarctic Pacific: importance of algal sinking and mesozooplankton herbivory. Deep-Sea Research II 46, 2669–2697.

Thomas, F., Minster, J.-F., Gaspar, P., Grégoris, Y., 1993. Comparing the behaviour of two ocean surface models in simulating dissolved oxygen concentration at Ocean Weather Station P. Deep-Sea Research 40, 395–408.

Tortell, P., Maldonado, M.T., Price, N.M., 1996. Iron limitation of marine heterotrophic bacteria. Nature 383, 330–332.

Varela, D.E., Harrison P.J., 1999. Seasonal variability in the nitrogenous nutrition of phytoplankton assemblages in the northeastern subarctic Pacific Ocean. Deep-Sea Research II 46, 2505–2538.

Vézina, A.F., Savenkoff, C., 1999. Inverse modelling of carbon and nitrogen flows in the pelagic food web of the northeast subarctic Pacific. Deep-Sea Research II 46, 2909–2939.

Webb, W.L., Newton, M., Starr, D., 1974. Carbon dioxide exchange of *Alnus rubra*: a mathematical model. Ecologia 17, 281–291.

Welschmeyer, N.A., Strom, S., Goericke, F., DiTullio, G., Belvin, M., Petersen, W., 1993. Primary production in the subarctic Pacific Ocean: project SUPER. Progress in Oceanography 32, 101–135.

Wheeler, P.A., 1993. New production in the subarctic Pacific Ocean: net changes in nitrate concentrations, rates of nitrate assimilation and accumulation of particulate nitrogen. Progress in Oceanography 32, 137–161.

Wheeler, P.A., Kokkinakis, S.A., 1990. Ammonium recycling limits nitrate use in the oceanic subarctic Pacific. Limnology and Oceanography 35, 1267–1278.

Whitney, F.A., Freeland, H.J., 1999. Variability in upper-ocean water properties in the NE Pacific Ocean. Deep-Sea Research II 46, 2351–2370.

Wong, C.S., 1989. Recent advances in remote observational systems and their applications in the open ocean environment. Marine Mining 8, 83–90.

Wong, C.S., Whitney, F.A., Iseki, K., Page, J.S., Zeng, Jiye, 1995. Analysis of trends in primary productivity and chlorophyll-*a* over two decades at Ocean Station P (50°N, 145°W) in the subarctic Northeast

Pacific Ocean. In: Beamish, R.J. (Ed.), Climate Change and Northern Fish Populations. Spec. Publ. Can. Fish. Aquat. Sci., Vol. 121, (pp. 107–117).

Wong, C.S., Whitney, F.A., Crawford, D.W., Iseki, K., Matear, R.J., Johnson, W.K., Page, J.S., Timothy, D., 1999. Seasonal and interannual variability in particle fluxes of carbon, nitrogen and silicon from time series of sediment traps at Ocean Station P, 1982–1993: relationships to subarctic primary productivity. Deep-Sea Research II 46, 2735–2760.

Woods, J.D., Barkmann, W., 1986. The response of the upper ocean to solar heating, I. The mixed layer. Quarterly Journal of the Royal Meteorological Society 112, 1–27.

Zahariev, K., 1998. Dynamics and modelling of the oceanic surface boundary layer: processes, sensitivities, implications, and parameterizations. Ph.D. dissertation, University of Victoria, Canada, 131 p.